NASA Technical Memorandum 78664

Control-Surface Hinge-Moment Calculations for a High-Aspect-Ratio Supercritical Wing

Boyd Perry III

SEPTEMBER 1978

NASA

NASA Technical Memorandum 78664

Control-Surface Hinge-Moment Calculations for a High-Aspect-Ratio Supercritical Wing

Boyd Perry III
Langley Research Center
Hampton, Virginia

National Aeronautics
and Space Administration

Scientific and Technical Information Office

1978

SUMMARY

An analytical investigation has been conducted to estimate the hinge moments, at selected flight conditions, resulting from deflecting two trailing-edge control surfaces (one inboard and one midspan) on a high-aspect-ratio, swept, fuel-conservative wing with a supercritical airfoil. This report gives hinge-moment results obtained from procedures which employ a recently developed transonic analysis. In this procedure a three-dimensional inviscid transonic aerodynamics computer program is combined with a two-dimensional turbulent-boundary-layer program in order to obtain an interacted solution. These results indicate that trends of the estimated hinge moment as a function of deflection angle are similar to those from experimental hinge-moment measurements made on wind-tunnel models with swept supercritical wings tested at similar values of free-stream Mach number and angle of attack.

INTRODUCTION

The Drones for Aerodynamics and Structural Testing (DAST) Project is a NASA flight program which uses a modified Firebee II target drone vehicle as a test-bed aircraft for testing aeroelastic research wings (ARW). In the integrated design of the second wing (designated ARW-2), the structural integrity of the wing depends on the successful operation of several active control systems. The ARW-2 design includes active controls for maneuver load alleviation (MLA), gust load alleviation (GLA), and flutter suppression (FS). All of these active control systems use trailing-edge control surfaces either to reduce or to redistribute the aerodynamic loads on the wing.

As part of the preliminary design of the hydraulic actuation system, which will be used to deflect these control surfaces, it was necessary to estimate the maximum control-surface hinge moments at critical design conditions. Therefore, hinge-moment calculations were made for two selected trailing-edge control surfaces using two iteratively interacted computer programs: a recently developed three-dimensional transonic aerodynamics computer program (refs. 1 and 2) and a two-dimensional turbulent boundary-layer computer program (refs. 3, 4, and 5). The procedure employed in interacting these programs is described in reference 6. The control surfaces analyzed represent an inboard surface intended for use with both the MLA and GLA systems and a midspan surface which was a candidate surface for the GLA system. The hinge moments were calculated for one control surface deflected at a time, and each control surface was analyzed at a separate flight condition. The hinge moments for the inboard surface were calculated at the design condition for the GLA system (the condition which sizes the hydraulic actuator). The hinge moments for the midspan surface were calculated at the design-cruise flight condition. The study was limited to one flight condition for each surface.

This paper presents the results of an analytical investigation to estimate the control-surface hinge moments for two control surfaces (one inboard and one

midspan) on a high-aspect-ratio supercritical wing. Two trailing-edge-down deflections, zero deflection, and one trailing-edge-up deflection were analyzed for each control surface. This paper includes (1) a brief discussion of the analytical methods used; (2) presentation of chordwise pressure distributions and spanwise load distributions at the four deflection angles for both control surfaces; (3) plots of hinge moment and total wing lift as a function of deflection angle for both control surfaces; and (4) a comparison of results with experimental data.

SYMBOLS

Values are given in both SI and U.S. Customary Units. Calculations were made in U.S. Customary Units.

b	wing span, m (ft)
C_h	hinge-moment coefficient, $H/q_\infty S_f c_{av}$
C_L	wing lift coefficient
C_p	pressure coefficient
c	local wing chord, m (ft)
c_{av}	average control-surface chord, m (ft)
c_l	section lift coefficient
c^*	product of local wing chord and cosine of local surface slope angle, m (ft)
g	acceleration due to gravity, 9.80 m/sec^2 (32.2 ft/sec^2)
H	hinge moment, positive for down load, N-m (in-lb)
h	hinge moment per unit span, positive for down load, N (lb)
M_∞	free-stream Mach number
q_∞	free-stream dynamic pressure, Pa (lb/in^2)
R	Reynolds number per meter (per foot)
S_f	control-surface area, m^2 (ft^2)
x	chordwise dimension, m (ft)
x_h	chordwise location of hinge, m (ft)
x_{te}	chordwise location of trailing edge, m (ft)

y spanwise dimension, m (ft)

α angle of attack, deg

δ control-surface deflection angle, positive trailing edge down, deg

δ^* boundary-layer displacement thickness, m (ft)

$\bar{\delta}^*$ relaxed boundary layer

Subscripts:

i current iteration (see fig. 2)

l lower surface

u upper surface

CONFIGURATIONS AND ANALYSIS CONDITIONS

The wing analyzed in this paper is fuel-conservative; that is, one with a high aspect ratio, moderate sweep angle, and supercritical airfoil. The geometric properties of the wing are listed in table I. For the study described in this paper, two trailing-edge control surfaces were analyzed, each at a different flight condition. Figure 1 shows the relative sizes and locations of both the inboard and midspan control surfaces. The following sections and table II describe the geometry of each control surface and the flight conditions at which the control-surface hinge moments were calculated.

Inboard Control Surface

The selected inboard control surface is indicated in figure 1(a). The control surface has a chord of 15 percent of the local wing chord (which includes the trailing-edge extension) and a span of 15 percent of the wing semispan; it extends from 12.5 percent to 27.5 percent of the semispan. The flight condition chosen for calculating the hinge moments for the inboard control surface is the design condition for the GLA system. The Mach number and altitude are 0.60 and 2134 m (7000 ft), respectively, conditions which result in a dynamic pressure of 19.70 kPa (411.3 psf) and a Reynolds number of 1.15×10^7 per meter (3.52×10^6 per foot). The angle of attack is 1.63°, which is the angle of attack required for a 2.5g pull-up maneuver at a vehicle gross weight of 11 121 N (2500 lb). The control-surface deflection angles selected for the investigation were $\delta = -5°$, 0°, 5°, and 10°.

Midspan Control Surface

The selected midspan control surface is indicated in figure 1(b). It had a chord of 20 percent of the local wing chord, a span of 25 percent of the wing semispan, and extended from 47.5 percent to 72.5 percent semispan. The flight

condition chosen for calculating the hinge moments for the midspan control surface is the design-cruise flight condition. The Mach number and altitude are 0.80 and 14 021 m (46 000 ft), respectively; these conditions result in a dynamic pressure of 6.312 kPa (131.8 psf) and a Reynolds number of 3.74×10^6 per meter (1.14×10^6 per foot). The angle of attack is 1.10°, which is the angle of attack required for 1g level flight at a wing lift coefficient of 0.53. The control-surface deflection angles selected for the investigation were $\delta = -5°$, 0°, 5°, and 12°.

ANALYTICAL METHODS

Two computer programs were employed in performing the analysis described in this paper: an aerodynamics program and a boundary-layer program. The procedure for interacting these two programs had been developed (ref. 6) in order to estimate (1) the angle of attack required for the wing at the design-cruise flight condition and (2) the resulting detailed load distributions for the basic wing without control surfaces. The reasonable agreement of these predictions with experimental data obtained subsequently encouraged the present application for control surfaces.

The aerodynamics program (FLO 22, refs. 1 and 2) analyzes inviscid, isentropic, transonic flow past three-dimensional swept-wing configurations. No provisions are included for modeling a fuselage. FLO 22 calculates chordwise pressure distributions on both the upper and lower surfaces of the wing. For a fine-grid computational mesh ($192 \times 24 \times 32$), 21 stations are used along the semispan (stations are spaced in increments of 5 percent semispan, starting at the root). The following description of the program is taken from the summary of reference 2: "The free-stream Mach number is restricted only by the isentropic assumption. Weak shock waves are automatically located wherever they occur in the flow. The finite-difference form of the full equation for the velocity potential is solved by the method of relaxation, after the flow exterior to the airfoil is mapped to the upper half plane. The mapping procedure allows exact satisfaction of the boundary conditions and use of supersonic free-stream velocities. The finite-difference operator is 'locally rotated' in supersonic flow regions so as to properly account for the domain of dependence. The relaxation algorithm has been stabilized using criteria from a time-like analogy."

The boundary layer is calculated using the two-dimensional integral-method boundary-layer formulation of Nash and Macdonald (ref. 3). The specific program used was extracted from a recent two-dimensional airfoil analysis program (ref. 4) and is basically the same as the boundary-layer program (NASHMAC) found in the airfoil program described in reference 5. NASHMAC calculates the boundary-layer displacement thickness along streamwise-oriented strips at 11 stations on the semispan. These 11 stations are, for convenience, picked from among the 21 output stations of FLO 22. Experience indicates that the boundary-layer calculation should begin in front of the assumed transition in order to approximate the laminar boundary-layer thickness. The locations for the start of the boundary-layer calculations are the same for both the upper and lower surfaces on the wing. Table III shows, for three stations along the span, the chordwise locations of the assumed transition (based on oil-flow

photographs from a similar configuration) and the start of the boundary layer. These locations varied linearly along the span in two segments: from the root to 42.6 percent semispan and from 42.6 percent semispan to the tip.

Assumptions and Limitations

Although the iterative-interactive procedure was used to investigate the effects of deflecting trailing-edge control surfaces, the procedure (ref. 6) was not developed specifically for that application. Consequently, some theoretical assumptions are less valid when the procedure is used to analyze deflected control surfaces. There are other assumptions which are less valid when the flight condition is changed from the design-cruise flight condition. As was stated earlier, the purpose of this paper is to provide analytical estimates of control-surface hinge moments. It is believed that none of the assumptions and limitations in the procedure are severe enough to alter trends or cloud results, and it is believed also that the purpose of performing these calculations was met. A brief discussion of the major assumptions and limitations follows.

Wing flexibility.- Because the wing used in this analysis is a high-aspect-ratio highly flexible wing, the effects of wing flexibility should be considered when the wing is analyzed at off-design flight conditions. However, because of the preliminary status of the ARW-2 integrated design, estimations of the wing shape (in the form of airfoil coordinates) at off-design conditions were not yet available. As a result, the wing shape used for all cases in this paper was the design-cruise shape. It is assumed that the differences in the pressure distributions (especially in the neighborhood of the control surfaces) caused by the differences between the off-design and design shapes are small. It is also assumed that the differences in control-surface hinge moments due to these small differences in pressure distributions are small.

Boundary layer.- Assumptions have been made regarding the method used to include viscous effects in this analysis. The two most important are (1) the two-dimensional boundary-layer displacement thicknesses calculated by NASHMAC adequately represent the actual three-dimensional boundary layer and (2) the empirically determined monotonic condition and the empirical separation criterion within NASHMAC still apply when the airfoil has a deflected control surface.

Iteration Procedure

The aerodynamics and boundary-layer computer programs are run in an iterative-interactive fashion, with the output of each one used as the input to the other one. The details of this application differ somewhat from those cited in reference 6. For example, in the present procedure the angle of attack was held constant. The first (inviscid) iteration starts and ends with a single running of FLO 22. Succeeding iterations start with the running of NASHMAC and end with the running of FLO 22. Iterations stop, and the solution is considered converged, when the total lift coefficient on the wing is within 1 percent of the lift coefficient from the previous iteration. For the relaxation scheme

used, the lift coefficient was found to decrease with each successive iteration, so that convergence is reached when $C_{L,i} > 0.99C_{L,i-1}$. A detailed description of the iteration procedure is illustrated in figure 2 and described in this section.

To start the first iteration, the airfoil coordinates at the 11 defining stations are used as input to FLO 22. The output from FLO 22 (completing the first iteration) consists of chordwise pressure distributions (referred to collectively as $C_{p,1}$) at the 21 output stations and the total lift coefficient of the wing ($C_{L,1}$).

To start the second iteration, the $C_{p,1}$ are used as input to NASHMAC. The output from NASHMAC consists of the boundary-layer displacement thicknesses (referred to collectively as δ_1^*) at the 11 defining stations. Within this iteration, the δ_1^* values are then multiplied by a weighting (relaxation) factor of 0.25, after which they are referred to as the relaxed boundary layer ($\bar{\delta}_1^*$). The relaxed boundary layer ($\bar{\delta}_1^*$) is then added to the original airfoil coordinates at the 11 defining stations, resulting in new airfoil coordinates which are used as input to FLO 22. The output of FLO 22 (completing the second iteration) consists of the new chordwise pressure distributions ($C_{p,2}$) and the new lift coefficient ($C_{L,2}$)

If the convergence criterion is not met, the third iteration starts with the $C_{p,2}$ used as input to NASHMAC. The output from NASHMAC, again, consists of new boundary-layer displacement thicknesses (δ_2^*) at the 11 defining stations. For this iteration, the new boundary-layer displacement $\bar{\delta}_2^*$ is a weighted average of δ_2^* with $\bar{\delta}_1^*$ according to the following (relaxation) scheme:

$$\bar{\delta}_2^* = 0.25 \times \delta_2^* + 0.75 \times \bar{\delta}_1^*$$

(This form of weighted average, combining the δ_i^* of the current iteration with the $\bar{\delta}_{i-1}^*$ from the previous iteration, is used in all successive iterations.) Then $\bar{\delta}_2^*$ is added to the original airfoil coordinates at the 11 defining stations, resulting in modified airfoil coordinates which are used as input to FLO 22. The output of FLO 22 (completing the third iteration) consists of the new chordwise pressure distributions ($C_{p,3}$) and the new lift coefficient ($C_{L,3}$).

The procedure described in the previous paragraph is repeated until the convergence criterion is met. When the convergence criterion is met, the control-surface hinge moments are calculated by integrating the product of the appropriate moment arm and the chordwise pressure distributions at those output stations corresponding to the control-surface location.

Hinge-Moment Calculation

Control-surface hinge moments are obtained in two steps: (1) chordwise integrations of the products of pressure distributions and appropriate moment arms to obtain a distribution of hinge moments per unit span; (2) a spanwise integration to obtain the total hinge moment. Both integration steps employed

a trapezoidal numerical integration. The limits of the chordwise integration are from the hinge line to the trailing edge. The hinge moment per unit span h is

$$h = q_\infty \int_{x_h}^{x_{te}} (C_{p,u} - C_{p,l})(x - x_h)\, dx$$

For a given control surface and a given deflection angle, repeated operations of this type result in hinge moments per unit span at stations within and immediately inboard and outboard of the spanwise extent of the control surface as shown in the following sketch:

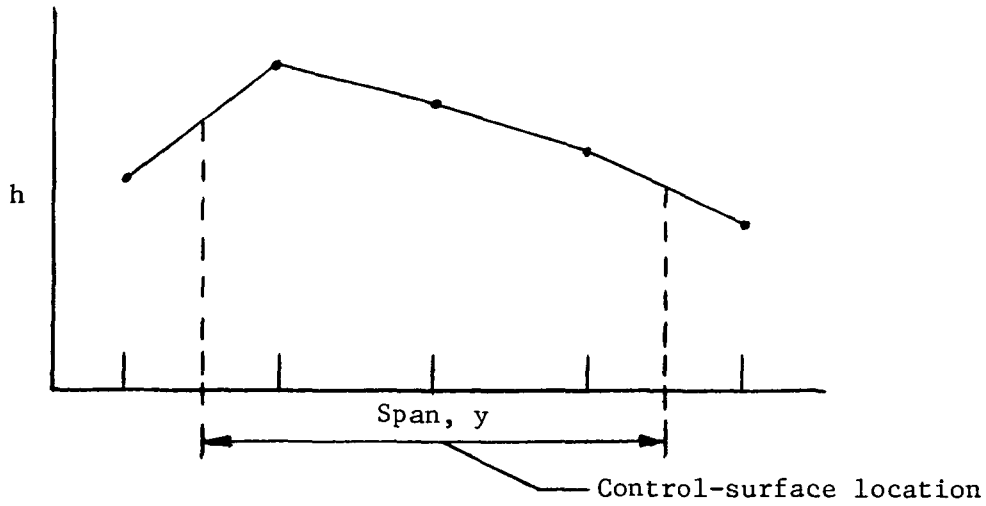

Because the inboard and outboard edges of the control surface lie between output stations, the values of h at these locations must be interpolated. The form of the spanwise integration is

$$H = \int_{y_{inboard}}^{y_{outboard}} h\, dy$$

Control-surface hinge moments are nondimensionalized by the product of the area and average chord of the control surface and the free-stream dynamic pressure to give

$$C_h = \frac{H}{q_\infty S_f c_{av}}$$

RESULTS AND DISCUSSION

This section contains analytical results and comparisons of some of the results with experiment.

Analytical Results

The following results are presented for each control surface: chordwise pressure distributions and chordwise boundary-layer displacement thicknesses for each control-surface deflection angle, spanwise load distributions with the deflection angle as a parameter, and plots of hinge-moment coefficient and lift coefficient as functions of control-surface deflection angle.

Inboard control surface.- Chordwise pressure distributions along the center line $\left(\frac{y}{b/2} = 0.20\right)$ of the control surface are presented in figure 3 for each deflection angle. The + symbols represent the pressures on the upper surface and the × symbols represent the pressures on the lower surface. The abscissa of each plot contains a sketch of the airfoil shape at $\frac{y}{b/2} = 0.20$ and includes the boundary layer and the deflected control surface. The hinge location is indicated by the dashed line on both the sketch and the pressure distribution. Figure 3 contains a typical representation of chordwise pressure distributions within the spanwise extent of the control surface and illustrates the effect on the pressures of changing the deflection angle. As expected, the lifting pressures increase with increasing deflection angle. For the three nonzero deflection angles, there are obvious kinks in the pressure distributions which occur at the points of discontinuity in slope on the upper and lower surfaces of the airfoil; that is, at the hinge location.

Plots of boundary-layer displacement thickness as a function of x/c for both the upper and lower surfaces at $\frac{y}{b/2} = 0.20$ are contained in figure 4. The displacement thicknesses have been nondimensionalized by the product of the local wing chord and the cosine of the local surface slope angle. The boundary layer on the upper surface becomes thicker at the trailing edge as the control-surface deflection angle is increased. As the deflection angle increases, so does the effective section camber. This increase accounts for the more pronounced peak in the displacement thickness on the lower surface. Examination of the output from the boundary-layer program indicates that the parameter which predicts possible flow separation had reached its threshold value for the two positive deflection angles. Thus flow separation and the accompanying loss of lift may occur at either of the two positive deflection angles.

Spanwise load distributions are presented in figure 5 for the four deflection angles of the investigation. The quantity cc_l is the product of the local chord and the section lift coefficient (the integral of the chordwise pressure distributions), and within the neighborhood of the control surface,

cc_l exhibits the same trends as the hinge moments per unit span (the integral of the product of the chordwise pressure distributions and the appropriate moment arms). Within the spanwise extent of the control surface there is a greater than 50-percent increase in cc_l in going from $\delta = -5^o$ to $\delta = 10^o$. Even though the control surface is located well inboard and is only 15-percent-semispan wide, the effect of deflecting the control surface is felt over the entire semispan.

Plots of hinge-moment coefficient and lift coefficient as functions of control-surface deflection angle are contained in figure 6. On the right side of the hinge-moment coefficient plot are scales indicating the dimensional values of the hinge moment in units of N-m and in-lb. The scale on the left side of the same plot has zero at the top of the scale and increases negatively down the scale. The results in figure 6 indicate that in going from $\delta = -5^o$ to $\delta = 10^o$, the total lift increases 25 percent, but the increase is achieved at the expense of an almost 140-percent increase in hinge moment.

Midspan control surface.- Chordwise pressure distributions along the center line $\left(\frac{y}{b/2} = 0.60\right)$ of the control surface are presented in figure 7. The hinge location is indicated by the dashed line. The higher Mach number and changes in airfoil shape account for distinct differences between these pressure distributions and those for the inboard control surface - the existence of a shock wave on the upper surface of the wing, for example. For the -5^o deflection, the shock wave is located at about 35 percent chord and is evidenced by the abrupt decrease in suction pressures on the upper surface at that location. The shock wave moves aft with increasing deflection angle, and the calculations indicate that, for the 12^o deflection, the shock wave moves onto the control surface. (The presence of the shock wave on the control surface could lead to problems such as loss of control-surface effectiveness and control-surface buzz.) The pressure distributions for all deflection angles exhibit similar kinks at the hinge location, and the lifting pressures increase with increasing deflection angle.

Plots of boundary-layer displacement thickness as a function of x/c for both the upper and lower surfaces at $\frac{y}{b/2} = 0.60$ are contained in figure 8. The boundary layers for the midspan control surface exhibit the same trends as those for the inboard control surface. They become thicker with increasing deflection angle, and they are significantly thicker than indicated for the inboard surface due, in part, to a two-thirds reduction in Reynolds number. In addition, the parameter which predicts possible flow separation reached its threshold value earlier along the chord than it did for the inboard control surface. This condition indicates possible separation at a chordwise location closer to the leading edge of the control surface.

Spanwise load distributions are presented in figure 9 for the four deflection angles of the investigation. Again, within the neighborhood of the control surface, cc_l exhibits the same trends as the hinge moments per unit span. The quantity cc_l increases by more than 100 percent in going from $\delta = -5^o$ to

$\delta = 12^{\circ}$. Because of its midspan location and increased span, the midspan control surface has a larger influence on the load distributions over the entire span than the inboard control surface does.

Plots of hinge-moment coefficient and lift coefficient as functions of control-surface deflection angle are contained in figure 10. In going from deflection angles of $\delta = -5^{\circ}$ to $\delta = 12^{\circ}$, the total lift increases 44 percent with a corresponding increase in hinge moment of over 100 percent. Although the hinge-moment coefficients are larger for the midspan control surface because of a significantly lower dynamic pressure, the actual hinge moments are only about half as large as those for the inboard control surface at all deflection angles.

Comparison With Experiment

The following discussion compares experimental measurements of control-surface hinge moments with the analytical results just presented. The measurements were obtained from wind-tunnel models with swept supercritical wings equipped with trailing-edge control surfaces.

Plots of experimental hinge-moment coefficients as functions of control-surface deflection angle are contained in figure 11 for the configurations reported in references 7 and 8. The planforms on the right side of the figure illustrate the relative locations and sizes of the control surfaces. The wing and control-surface geometry of both models differed from the geometry of the ARW-2 configuration (as illustrated in table IV), and they were tested at different (but similar) values of angle of attack and Mach number. Even with these differences, both the hinge-moment magnitudes ($-0.4 < C_h < 0$) and trends (C_h becomes more negative with increasing deflection angle) of the data in figure 11 are consistent with the analytical results presented in figures 6 and 10. However, the experimental measurements do exhibit a noticeable change in slope in going from negative to positive deflections, which the analysis of the ARW-2 configuration did not predict.

Figure 12 contains plots of measured and calculated hinge-moment coefficients for the ARW-2 configuration as functions of control-surface deflection angle. The calculations are those presented in figure 6 and the measurements were obtained from a recent wind-tunnel investigation conducted by Thomas A. Byrdsong in the Langley 8-foot transonic pressure tunnel. The investigation measured control-surface hinge moments on a rigid 0.237-scale model of the ARW-2 configuration with some candidate active-control surfaces. Results are for the inboard control surface at the same values of Mach number and angle of attack. These results show excellent agreement over the range of deflection angles used. There were no measurements made on the midspan control surface for comparison with the calculations presented in figure 10.

CONCLUDING REMARKS

An analytical investigation has been conducted to estimate the hinge moments resulting from deflecting two trailing-edge control surfaces (one inboard and one midspan) on a high-aspect-ratio, swept, fuel-conservative wing

with a supercritical airfoil. The results of this investigation indicate that within the spanwise extent of the control surfaces, the magnitudes of the chordwise pressure distribution aft of the hinge line increase with increasing control-surface deflection angle. In addition, due to the higher free-stream Mach number selected for the midspan control surface, the pressure distributions show the presence of a shock wave on the upper surface. For both control surfaces, the effect on the spanwise load distribution of deflecting the control surface is felt over the entire semispan, and significant local effects are felt in the neighborhood of the control surface. The trends of the estimated hinge moments as functions of deflection angle are consistent with experimental hinge-moment measurements made on wind-tunnel models with swept supercritical wings tested at similar values of free-stream Mach number and angle of attack. At the same free-stream Mach number and angle of attack, a comparison of the calculated hinge-moment coefficients with coefficients measured on a 0.237-scale model of the configuration analyzed showed excellent agreement over the range of deflection angles considered.

Langley Research Center
National Aeronautics and Space Administration
Hampton, VA 23665
July 28, 1978

REFERENCES

1. Jameson, Antony; and Caughey, D. A.: Numerical Calculation of the Transonic Flow Past a Swept Wing. NASA CR-153297, 1977.

2. Jameson, Antony; Caughey, David A.; Newman, Perry A.; and Davis, Ruby M.: A Brief Description of the Jameson-Caughey NYU Transonic Swept-Wing Computer Program - FLO 22. NASA TM X-73996, 1976.

3. Nash, J. F.; and Macdonald, A. G. J.: The Calculation of Momentum Thickness in a Turbulent Boundary Layer at Mach Numbers up to Unity. C.P. No. 963, British A.R.C., 1967.

4. Carlson, Leland A.: TRANDES: A FORTRAN Program for Transonic Airfoil Analysis or Design. NASA CR-2821, 1977.

5. Bauer, Francis; Garabedian, Paul; Korn, David; and Jameson, Antony: Supercritical Wing Sections II. Volume 108 of Lecture Notes in Economics and Mathematical Systems, Springer-Verlag, 1975.

6. Newman, Perry A.; Carter, James E.; and Davis, Ruby M.: Interaction of a Two-Dimensional Strip Boundary Layer With a Three-Dimensional Transonic Swept-Wing Code. NASA TM-78640, 1978.

7. Re, Richard J.: Stability and Control Characteristics, Including Aileron Hinge Moments, of a Model of a Supercritical-Wing Research Airplane. NASA TM X-2929, 1974.

8. Mann, Michael J.; and Langhans, Richard A.: Transonic Aerodynamic Characteristics of a Supercritical-Wing Transport Model With Trailing-Edge Controls. NASA TM X-3431, 1977.

TABLE I.- WING GEOMETRIC PROPERTIES

Aspect ratio	10.30
Taper ratio	0.400
Planform area, m^2 (ft^2)	3.25 (35)
Span, m (ft)	5.79 (18.99)
Mean aerodynamic chord, m (ft)	0.596 (1.96)
Sweep (0.50c), deg	25
Trailing-edge extension:	
At $\frac{y}{b/2} = 0$	0.400c
At $\frac{y}{b/2} = 0.426$	0
Thickness:	
At $\frac{y}{b/2} = 0.106$	0.144c
At $\frac{y}{b/2} = 0.426$	0.120c
At $\frac{y}{b/2} = 1.00$	0.106c
Twist, deg:	
At $\frac{y}{b/2} = 0.106$	2.0
At $\frac{y}{b/2} = 0.426$	-0.5
At $\frac{y}{b/2} = 1.00$	-1.6

TABLE II.- ANALYSIS CONDITIONS FOR SELECTED CONTROL SURFACES

Quantity	Control surface	
	Inboard	Midspan
Mach number, M_∞	0.60	0.80
Angle of attack, α, deg . . .	1.63	1.10
Altitude, m (ft)	2134 (7000)	14 021 (46 000)
Dynamic pressure, q_∞, kPa (lb/ft^2)	19.70 (411.3)	6.312 (131.8)
Reynolds number, R, m^{-1} (ft^{-1})	1.15×10^7 (3.52×10^6)	3.74×10^6 (1.14×10^6)
Deflection angles, δ, deg	-5, 0, 5, 10	-5, 0, 5, 12

TABLE III.- ASSUMED BOUNDARY-LAYER TRANSITION

Span station	Assumed transition, percent local chord	Boundary-layer start, percent local chord
Root (fuselage ¢)	10.6	8.5
42.6 percent semispan	30.0	24.0
Tip	10.0	8.0

TABLE IV.- COMPARISON OF CONFIGURATION GEOMETRY

Quantity	Configuration				
	ARW-2		Reference 7		Reference 8
Wing					
Aspect ratio	10.30		6.78		7.50
Taper ratio	0.400		0.364		0.418
Sweep (0.25c), deg . . .	27		42		33
Control surface					
Designation	Inboard	Midspan	1	2	3
Chord	0.150c	0.200c	0.250c	0.250c	0.219c
Span	0.150b/2	0.250b/2	0.200b/2	0.200b/2	0.102b/2

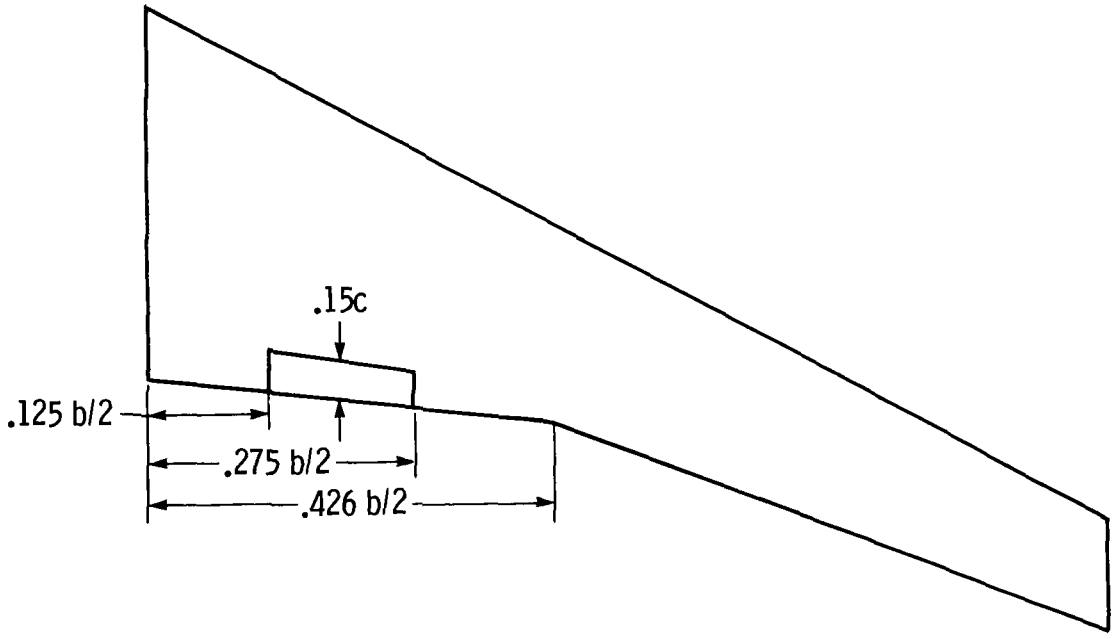

(a) Inboard control surface.

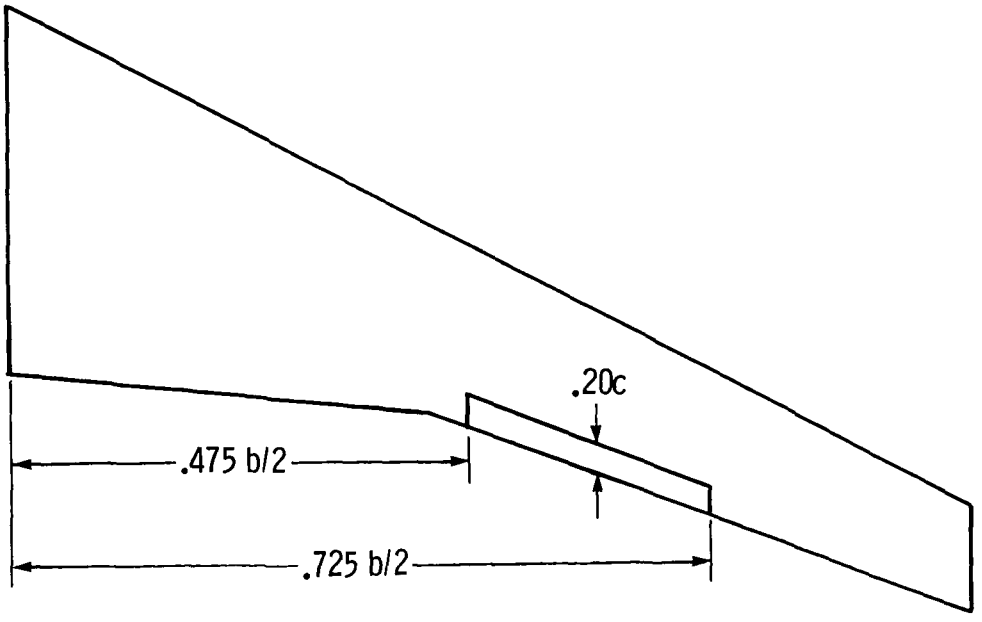

(b) Midspan control surface.

Figure 1.- Planform views of wing showing locations of selected trailing-edge control surfaces.

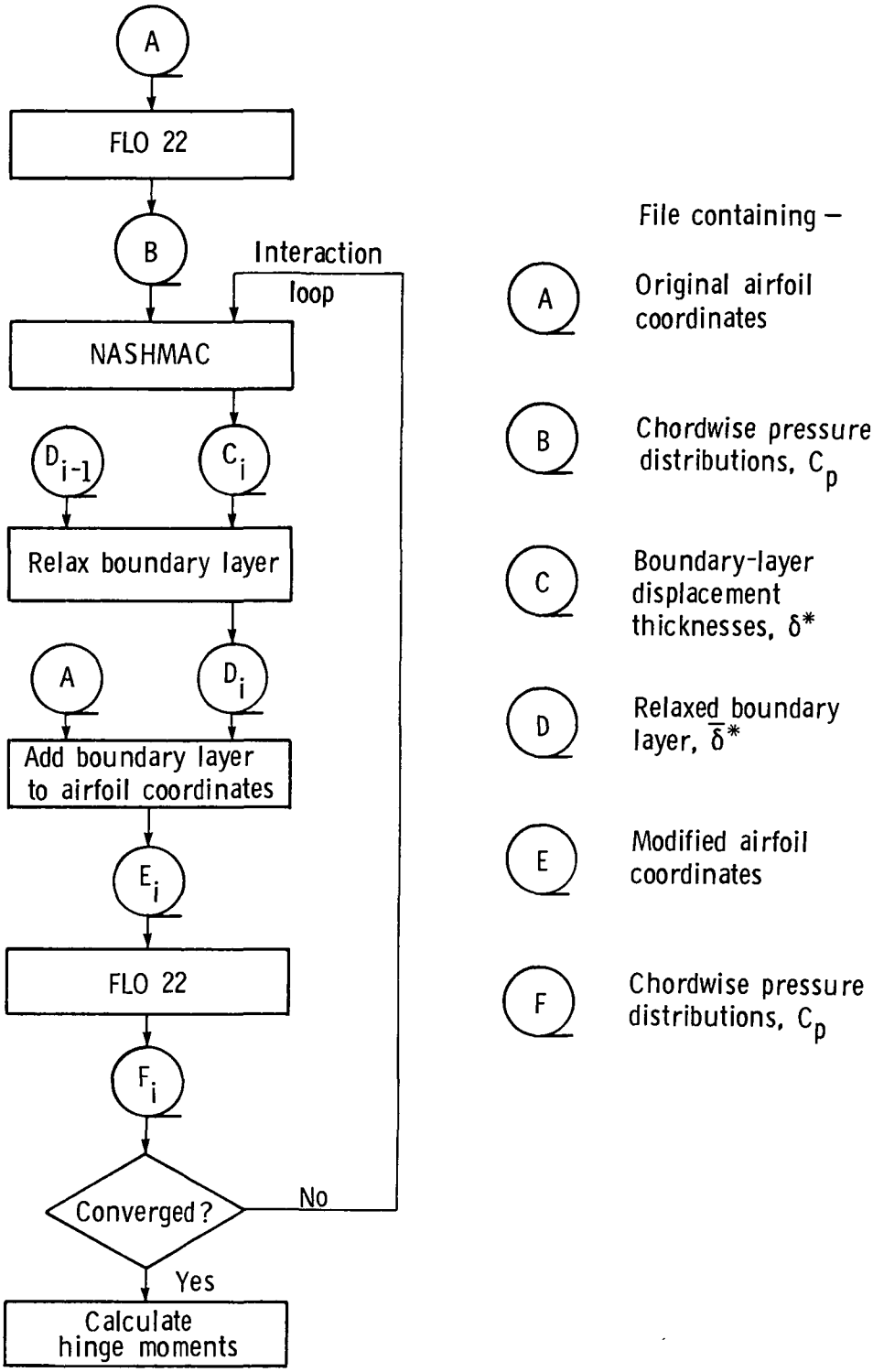

Figure 2.- Flow chart for iterative-interactive procedure. Subscripts i and i-1 refer to the current and previous iterations, respectively.

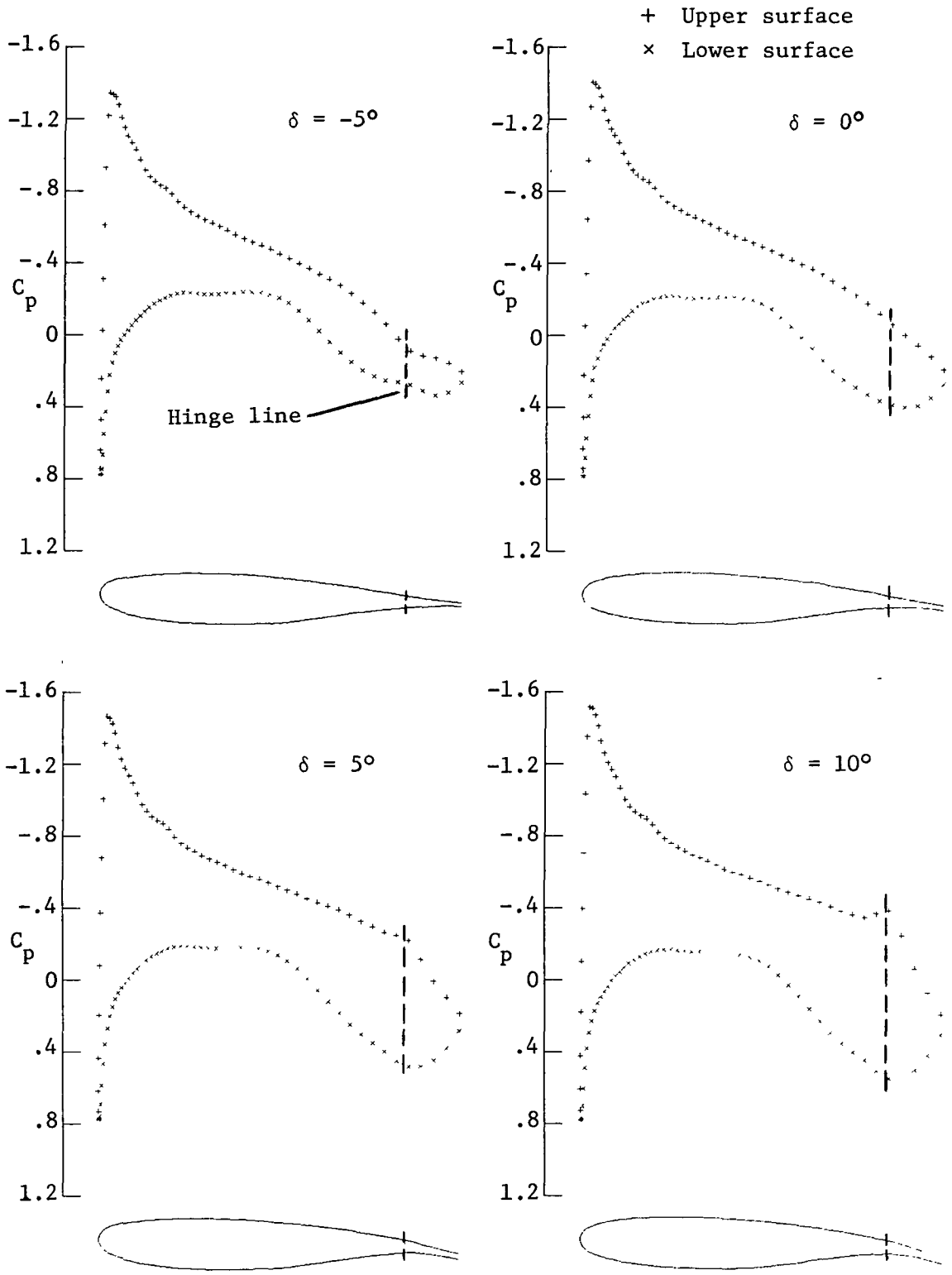

Figure 3.- Chordwise pressure distributions along center line $\left(\frac{y}{b/2} = 0.20\right)$ of inboard control surface. $M_\infty = 0.60$; $\alpha = 1.63^\circ$; $q_\infty = 19.70$ kPa (411.3 lb/ft^2).

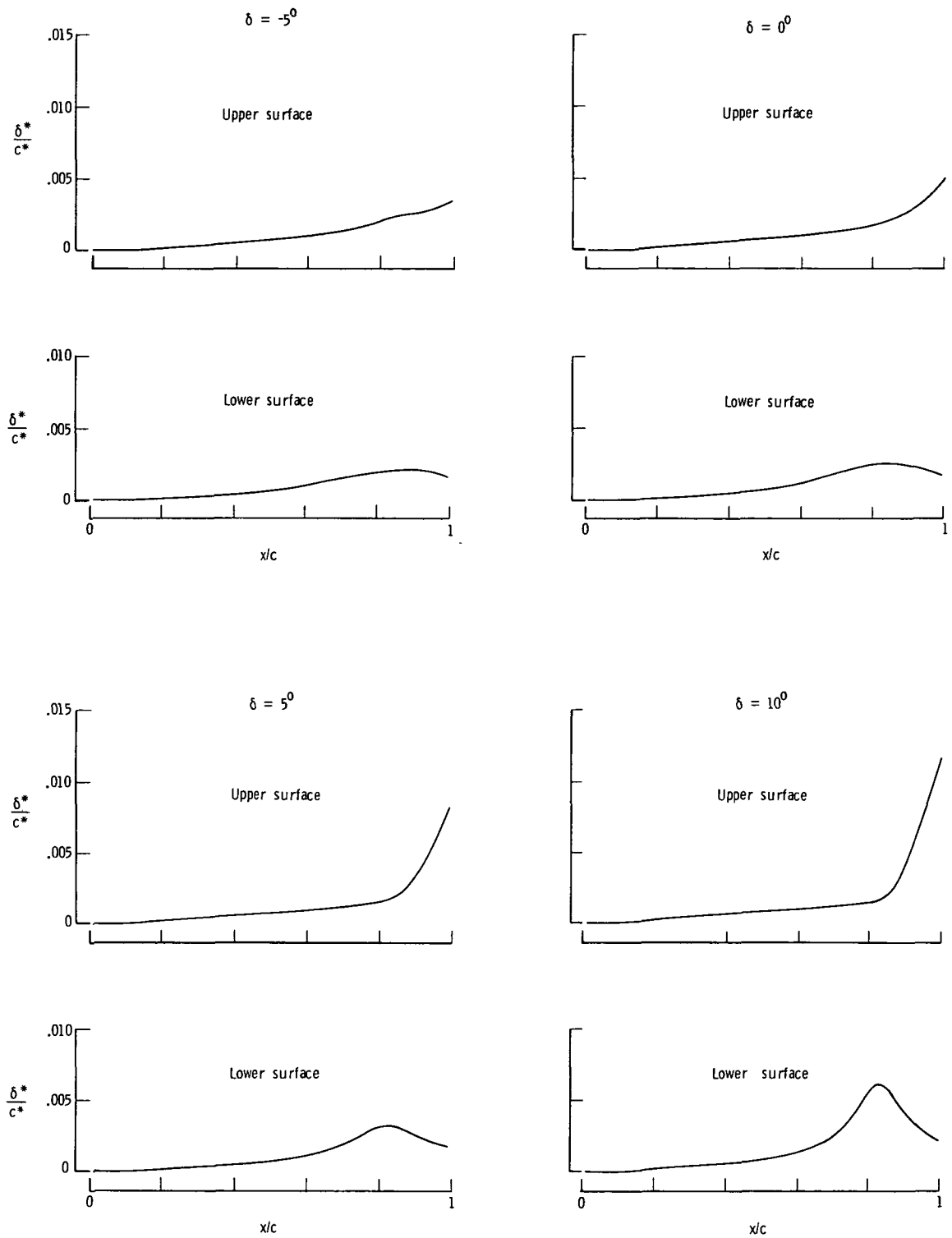

Figure 4.- Chordwise boundary-layer displacement thickness distributions along center line $\left(\frac{y}{b/2} = 0.20\right)$ of inboard control surface. $M_\infty = 0.60$; $\alpha = 1.63^\circ$; $q_\infty = 19.70$ kPa (411.3 lb/ft^2).

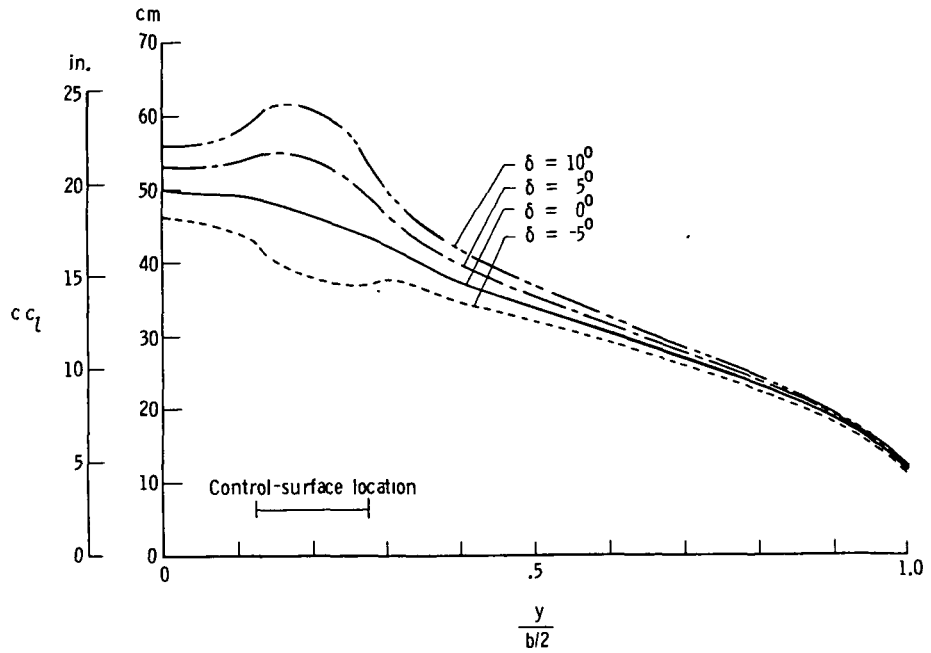

Figure 5.- Spanwise load distribution for inboard control surface deflected. $M_\infty = 0.60$; $\alpha = 1.63^o$; $q_\infty = 19.70$ kPa (411.3 lb/ft^2).

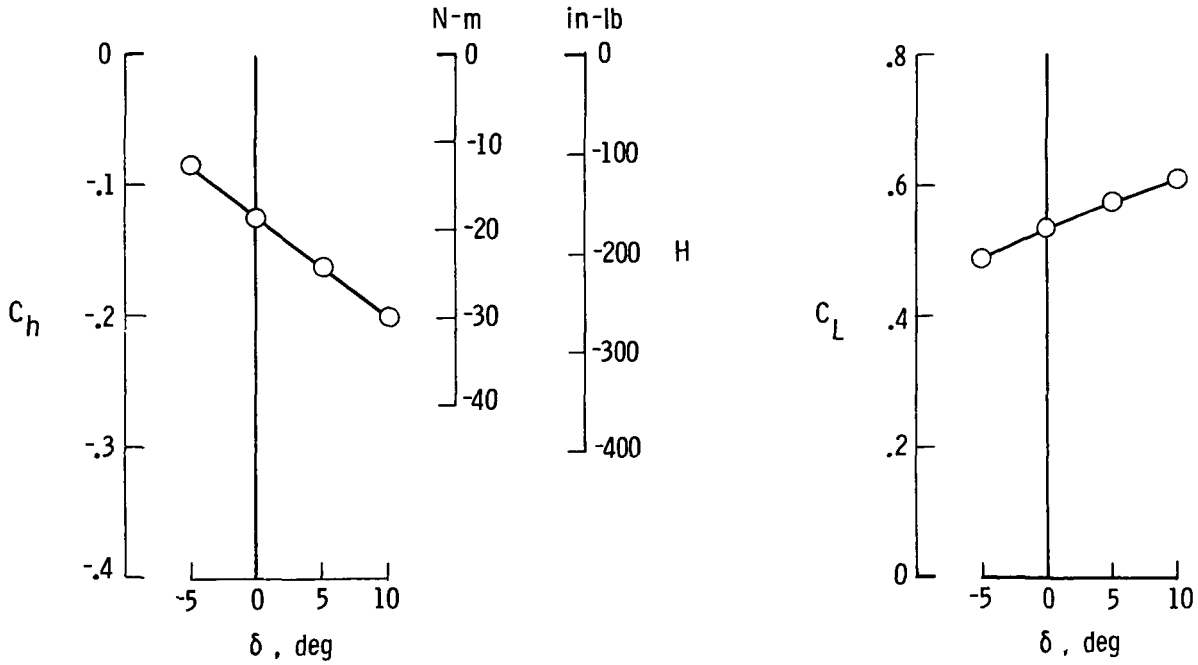

Figure 6.- Hinge-moment and lift coefficients for inboard control surface. $M_\infty = 0.60$; $\alpha = 1.63^o$; $q_\infty = 19.70$ kPa (411.3 lb/ft^2).

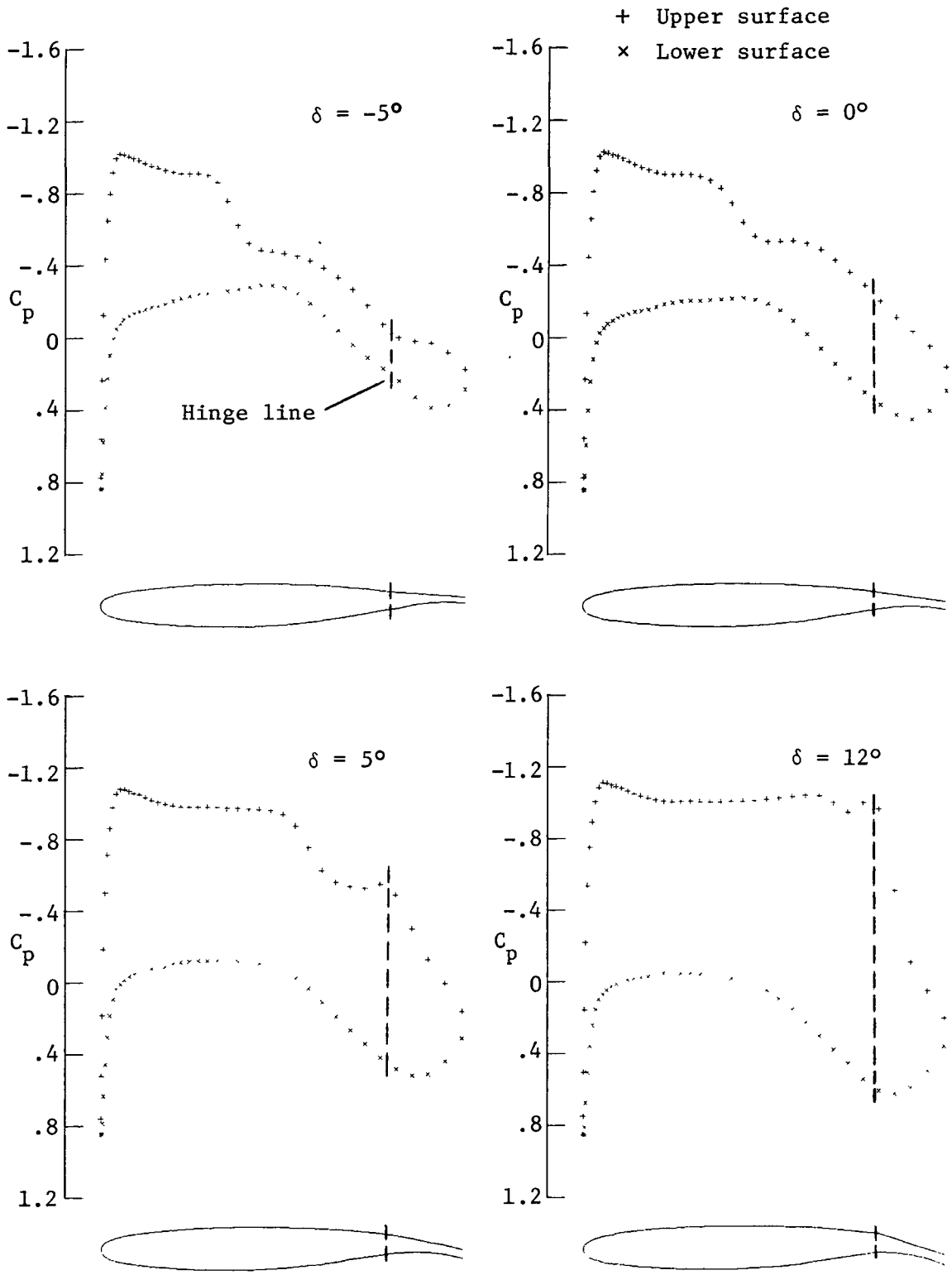

Figure 7.- Chordwise pressure distributions along center line $\left(\frac{y}{b/2} = 0.60\right)$ of midspan control surface. $M_\infty = 0.80$; $\alpha = 1.10^\circ$; $q_\infty = 6.31$ kPa (131.8 lb/ft^2).

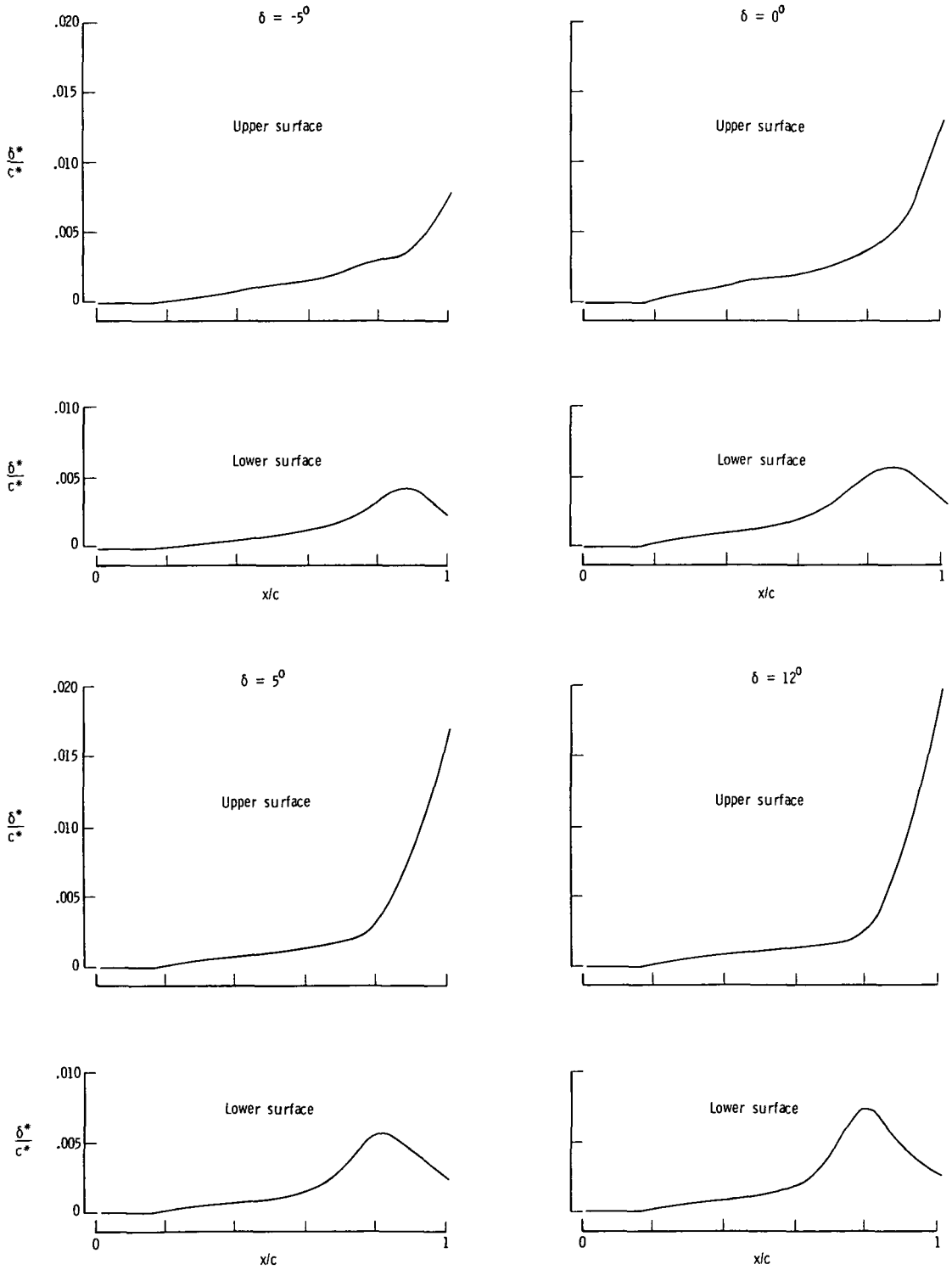

Figure 8.- Chordwise boundary-layer displacement thickness distributions along center line $\left(\frac{y}{b/2} = 0.60\right)$ of midspan control surface. $M_\infty = 0.80$; $\alpha = 1.10^\circ$; $q_\infty = 6.31$ kPa (131.8 lb/ft^2).

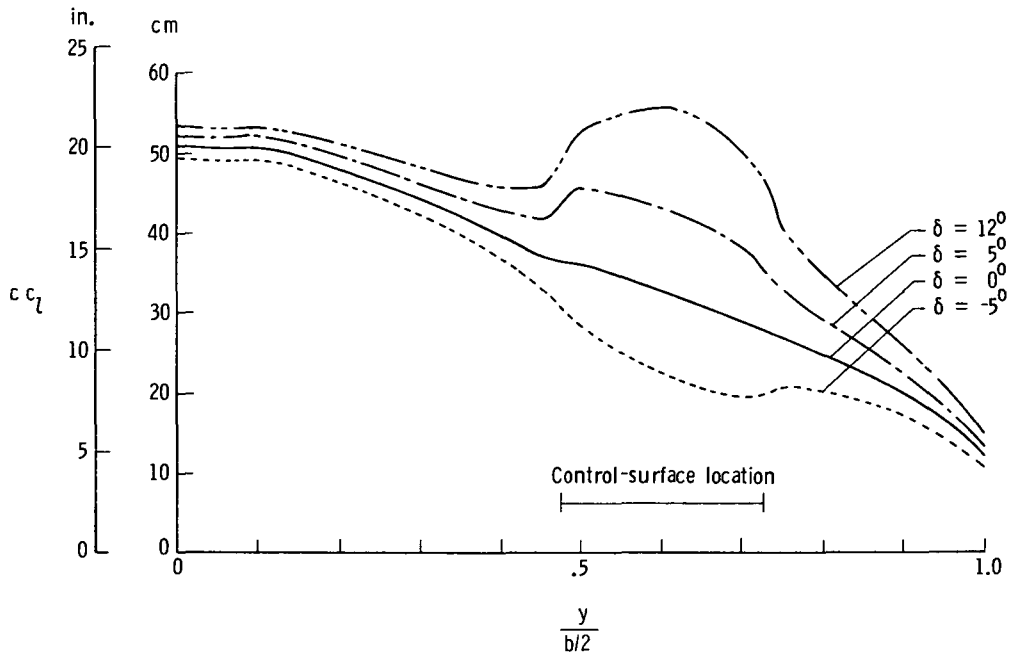

Figure 9.- Spanwise load distribution for midspan control surface deflected. M_∞ = 0.80; α = 1.10°; q_∞ = 6.31 kPa (131.8 lb/ft^2).

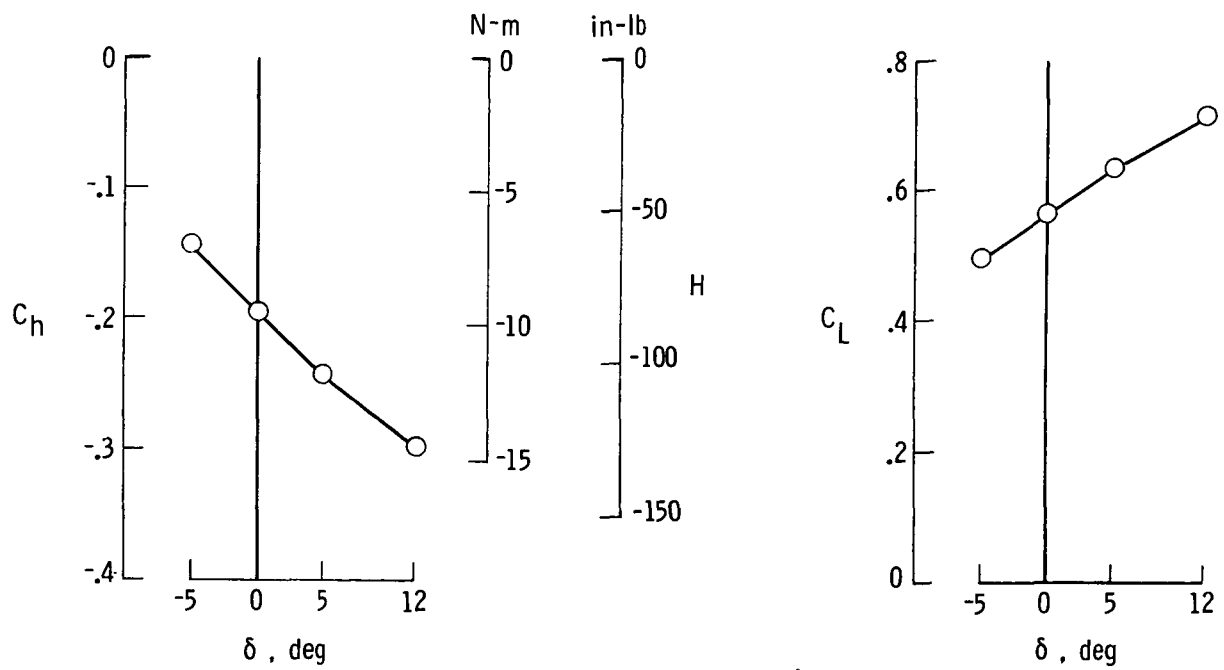

Figure 10.- Hinge-moment and lift coefficients for midspan control surface. M_∞ = 0.80; α = 1.10°; q_∞ = 6.31 kPa (131.8 lb/ft^2).

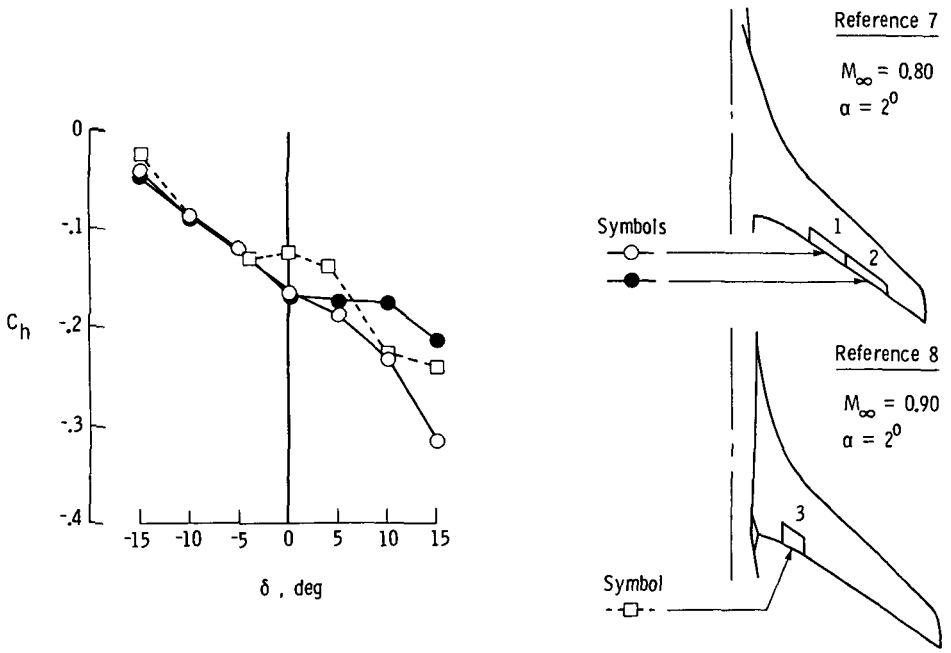

Figure 11.- Hinge-moment coefficient as a function of control-surface deflection angle for references 7 and 8.

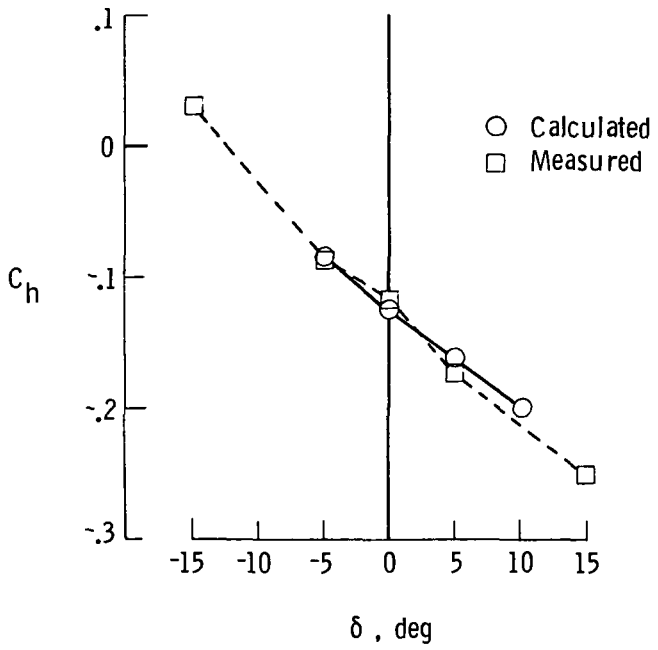

Figure 12.- Calculated and measured hinge-moment coefficients for inboard control surface. M_∞ = 0.60; α = 1.63°. (Measurements were obtained by Thomas A. Byrdsong in Langley 8-foot transonic pressure tunnel.)

1 Report No.	2 Government Accession No	3 Recipient's Catalog No
NASA TM-78664		

4 Title and Subtitle	5 Report Date
CONTROL-SURFACE HINGE-MOMENT CALCULATIONS FOR A HIGH-ASPECT-RATIO SUPERCRITICAL WING	September 1978
	6 Performing Organization Code
7 Author(s)	8 Performing Organization Report No
Boyd Perry III	L-12219
9 Performing Organization Name and Address	10. Work Unit No
NASA Langley Research Center Hampton, VA 23665	516-53-03-21
	11 Contract or Grant No
	13 Type of Report and Period Covered
12 Sponsoring Agency Name and Address	Technical Memorandum
National Aeronautics and Space Administration Washington, DC 20546	14 Sponsoring Agency Code

15 Supplementary Notes

16 Abstract

An analytical investigation has been conducted to estimate the hinge moments, at selected flight conditions, resulting from deflecting two trailing-edge control surfaces (one inboard and one midspan) on a high-aspect-ratio, swept, fuel-conservative wing with a supercritical airfoil. This report gives hinge-moment results obtained from procedures which employ a recently developed transonic analysis. In this procedure a three-dimensional inviscid transonic aerodynamics computer program is combined with a two-dimensional turbulent-boundary-layer program in order to obtain an interacted solution. These results indicate that trends of the estimated hinge moment as a function of deflection angle are similar to those from experimental hinge-moment measurements made on wind-tunnel models with swept supercritical wings tested at similar values of free-stream Mach number and angle of attack.

17 Key Words (Suggested by Author(s))	18 Distribution Statement
Transonic flow Compressible flow Control-surface hinge moments Trailing-edge controls	Unclassified - Unlimited Subject Category 02

19 Security Classif (of this report)	20 Security Classif (of this page)	21 No of Pages	22. Price*
Unclassified	Unclassified	23	$4.00

* For sale by the National Technical Information Service, Springfield, Virginia 22161

NASA-Langley, 1978

4 1 1U,A, 082178 S00673HU
NORTHROP UNIV
ATTN: ALUMNI LIBRARY
1155 WEST ARBOR VITAE ST
INGLEWOOD CA 90306